Assessment of climate change impact on wintertime meteorology over California using dynamical downscaling method with a bias correction technique

Zhan Zhao[1] · Pingkuan Di[1] · Shu-Hua Chen[2] · Jeremy Avise[1,3] · Ajith Kaduwela[1,4]

Abstract

Climate change can potentially have great impacts on wintertime precipitation and stagnant conditions, which are critical for both water resources and wintertime particulate matter (PM), in California. This study utilizes the Weather Research and Forecasting model to dynamically downscale a bias-corrected coarse-resolution global climate model dataset from the Coupled Model Intercomparison Project Phase 5 (CMIP5) to a grid size of 4×4 km^2 over California for a present (2003–2012) and a future (2046–2055) decade. Compared to the present climate, an increase in 2-m temperature (up to 2 K) and water vapor mixing ratio (up to 1 g/kg) and a decrease in planetary boundary layer height (up to 80 m) are projected by the 2050s for the entire state of California. The number of stagnant days over the San Joaquin Valley is expected to increase by approximately 6% in the future decade, indicating potential exacerbation of the winter PM issue in this region. The wintertime precipitation is projected to increase by up to 50% in northern California and, conversely, to decrease by up to 40% in southern California during 2046–2055. The solid phase precipitation is projected to decrease over mountain ranges with lower elevations despite an overall increase in total precipitation, while it is projected to increase over the eastern side of the Sierra Nevada with elevation over 2 km.

1 Introduction

California has a classic Mediterranean climate, and the major precipitation seasons are winter and early spring. The snowpack at high elevations, especially in the Sierra Nevada

✉ Zhan Zhao
zhan.zhao@arb.ca.gov

[1] Modeling and Meteorology Branch, Air Quality Planning and Science Division, Air Resources Board, California Environmental Protection Agency, Sacramento, CA, USA

[2] Department of Land, Air, and Water Resources, University of California, Davis, CA, USA

[3] Department of Civil and Environmental Engineering, Washington State University, Pullman, WA, USA

[4] Air Quality Research Center, University of California, Davis, CA, USA

mountains, is a vital water resource for all of California. During the following spring, the melting of the snowpack over the Sierra Nevada provides roughly 30% of the water supply for the state's water reservoirs and about 75% of the water supply to agricultural sectors in California's central valley (CV; Huang et al. 2018; Huning and AghaKouchak 2018). At lower elevations, abundant precipitation events over large areas can lead to flooding, which causes large adverse social and economic consequences. The wintertime precipitation and snowpack in California can be very sensitive to climate change (Swain et al. 2018).

Atmospheric Rivers (AR), which are narrow corridors of abundant water vapor in the lower troposphere that extend from the tropics to middle and high latitudes, have been identified as the leading contributor to the winter precipitation over California. ARs that make landfall in California have contributed from one third to one half of the state's total precipitation (Ralph and Dettinger 2011, 2012). However, storms associated with ARs are also linked to most of the largest floods in California (Ralph et al. 2006). Studies have projected a large increase in the number of days associated with ARs that approach the U.S. west coast by the end of the twenty-first century (Gao et al. 2015; Warner

et al. 2015). The orographic precipitation associated with the ARs leads to large snowpack accumulation over mountainous regions, such as the Sierra Nevada with high elevations, by the end of the spring. Climate warming will likely cause earlier snowpack melt in the springtime and reduce frozen precipitation, both of which will lead to declines in the amount and duration of the annual snowpack over the Sierra Nevada and will lead to conditions throughout the State that are more favorable to drought (Berg and Hall 2017). The Intergovernmental Panel on Climate Change (IPCC 2012) and other studies (Meehl et al. 2000; Coumou and Rahmstorf 2012) report increases in both the occurrence and intensity of weather extremes under a changing climate, which is reflected in the increase of precipitation extremes over California (Berg and Hall 2015; Swain et al. 2018). As an example, after an extraordinary drought that lasted from 2011 to 2015 (Berg and Hall 2017; Swain et al. 2014), California experienced an extremely wet winter which lasted from November 2016 to March 2017 associated with a number of ARs that broke the historical record going back to 1895 (Wang et al. 2017). California's winter precipitation and water resources are especially sensitive and vulnerable to climate change. Therefore, it is important to investigate the projected future changes in the wintertime precipitation over California, which is critical for the public policymakers to develop coherent strategies and responses for mitigating the effects of climate change.

In addition to precipitation in wintertime, California has been long recognized for its severe particulate matter (PM) problem in the winter months, which can be modulated by climate change. San Joaquin Valley (SJV), which is the southern part of the CV, is one of the largest $PM_{2.5}$ nonattainment areas in the United States (U.S.) that consistently exceeds both the national and state air quality standards (Chen et al. 2020). As stated in previous studies (Zhao et al. 2011b; Chen et al. 2014), meteorological conditions play a crucial role in the winter PM episodes over SJV.

PM has serious adverse health effects, and previous studies have shown a strong correlation between mortality and elevated PM concentrations (Dockery et al. 1993; Pope III and Dockery 2006). High PM concentration is also linked to impaired visibility (Eldering and Cass 1996). A semi-permanent Pacific Subtropical High (PSH) typically sits off the California coast. During winter, the PSH intrudes inland and stalls over the CV for a prolonged period of time, resulting in atmospheric stagnation with a shallow planetary boundary layer and a reduced planetary boundary layer height (PBLH) due to both subsidence and low wind speed. At nighttime, due to clear skies and calm winds, strong temperature inversions occur near the surface, further reducing vertical mixing. Both conditions are conducive to pollutant buildup within in the valley (Bao et al. 2008; Zhao et al. 2011b). Furthermore, these pollutants are trapped within the shallow boundary layer and the surrounding mountain ranges help to trap pollution within the valley. As a result, the stagnation conditions in SJV during winter are generally more severe compared to other regions over California, leading to high PM concentrations over this region. Previous studies project increases in the occurrence of stagnation associated with PSH over California in response to global warming (Horton et al. 2012, 2014; Zhao et al. 2011b; Leung and Gustafson 2005). Detailed and comprehensive analysis of the potential future changes in the stagnation over SJV will give policy makers insights on emission control strategy development for mitigating the effect of climate change on winter PM events, and the problems they incur, in the SJV.

Global climate model (GCM) simulations with relatively coarse spatial resolution are insufficient to adequately represent the mesoscale features and climate projections of the regional meteorology in California due to its proximity to the ocean, complex terrain, intricate mesoscale weather systems, and flow patterns. For instance, the aforementioned precipitation events associated with landfalling ARs are caused by orographic lifting from the mountainous terrain over California (Neiman et al. 2008a, b; Leung and Qian 2009); a regional model with high spatial resolution works better in resolving the complex orography and reproducing the orographic precipitation compared to a global model that usually uses a more coarse spatial resolution. Thus, to better represent topographic effects and regional meteorology in our climate simulations, the regional Weather Research and Forecasting model (WRF) is utilized to dynamically downscale the Community Earth System Model (CESM) simulation results from the Coupled Model Intercomparison Project Phase 5 (CMIP5; CMIP5; Taylor et al. 2012) under the representative concentration pathways 6.0 (RCP6.0) emission scenario to a horizontal grid size of 4×4 km^2 over California. The RCP6.0 emission scenario is believed to be most closely aligned with local climate solutions applied in California towards economic, social, and environmental sustainability with intermediate population increase and intermediate economic development (Zhao et al. 2020). The years of 2003–2012 and 2046–2055 were selected as the current and future climate periods, respectively. Prior to the dynamical downscaling process, a bias correction technique was applied to adjust both the climatological mean and the inter-annual variations of the CESM variables based on reanalysis data (Zhao et al. 2020). This bias correction method was shown to be superior than the conventional bias correction method, which only corrects the climatological means, in capturing weather extremes and improving probability distributions of meteorological variables of the downscaled results (Xu and Yang 2012, 2015; Zhao et al. 2020).

This paper is the second part of our California climate change study. The first part of the study, which was published in Zhao et al. (2020), focuses on (1) evaluating the

dynamical downscaling method with bias correction by comparing the WRF downscaled results driven by CESM data with and without bias correction for the present decade to WRF results driven by reanalysis data and observations, and (2) investigating the impact of climate change on meteorological variables that are crucial to summer ozone formation and on summertime atmospheric phenomena (e.g., heat wave, marine air penetration) by the 2050s in California. Zhao et al. (2020) reported an approximately 1 K increase in summertime mean 2-m temperature (T2) and an up to 0.6 g/kg increase in 2-m water vapor mixing ratio (Qv2) for the entirety of California by the 2050s. Both the frequency and duration of the heat wave events were projected to increase over California; future increases in the occurrence and intensity of marine air penetration were also projected.

This paper, the second part of our climate study, investigates (1) future climate change on meteorological variables that are crucial to winter PM episodes in California, including temperature, humidity, wind and PBLH, (2) projected future changes in wintertime precipitation and snowpack over California, as well as potential future changes in ARs that make landfalls in California, and (3) the impact of climate change on the stagnant conditions over the SJV. A considerable amount of wintertime precipitation is also received in March, thus the wintertime analysis in this study covers the months from December to March.

This paper is organized as follows. Section 2 describes the models, model configurations and the methodology applied in this study. Section 3 evaluates wintertime dynamical downscaling results for the present decade. Section 4 presents the projected future changes in wintertime meteorological parameters over California and different geographical sub-regions of the state. Section 5 discusses potential future changes on wintertime precipitation and AR activities over California. Section 6 analyzes the projected stagnation conditions over the SJV by the 2050s. Concluding remarks are given in Sect. 7.

2 Models and methodology

A detailed description of the models (CESM and WRF for GCM and RCM, respectively), and the dynamical downscaling method and bias correction technique used in this study, are provided in Zhao et al. (2020) and thus they are only briefly described here.

CESM is a fully-coupled global climate model developed by the National Center for Atmospheric Research (NCAR) and other institutes. For CMIP5, CESM is configured with a nominal horizontal grid of $0.9° \times 1.25°$ and 26 vertical levels. CESM CMIP runs include simulations of twentieth-century climate (1850–2005) and twenty-first-century climate (2005–2100) with four different RCP scenarios (i.e. RCP2.6,

RCP4.5, RCP6.0 and RCP8.5). There are six ensemble members for the twentieth-century climate and for each of the RCP scenarios for the twenty-first-century climate (Peacock 2012). In this study, future climates are based on results from the "medium–high emissions" (RCP6.0) scenario, which is believed to be better aligned with future emission planning in California. The climate model simulations used in this study are described in Meehl et al. (2012) and Peacock (2012) in great detail.

The WRF model with the Advanced Research WRF (ARW) dynamic core version 3.5.1 (Skamarock et al. 2008) is used in this study to downscale CESM results. WRF has been widely used to simulate different weather phenomena over California (Jankov et al. 2009; Leung and Qian 2009; Lu et al. 2012) and to dynamically downscale GCM results for different applications (Caldwell et al. 2009; Zhao et al. 2011a). The WRF model is configured with three nested domains with horizontal grid sizes of 36, 12, and 4 km, and with 31 vertical layers (Fig. 2a in Zhao et al. 2020). The WRF physics schemes used in this study include WRF Single-Moment 6-class (WSM6) microphysics (Hong and Lim 2006), Rapid Radiative Transfer Model (RRTM) longwave radiation (Mlawer et al. 1997), Dudhia short wave radiation (Dudhia 1989), Pleim–Xiu land-surface parameterization (Pleim and Xiu 1995), Yonsei University PBL parameterization (Hong et al. 2006), and Kain-Fritsch convective parameterization (Kain 2004) for the outer 2 domains. Spectral nudging is applied to temperature, horizontal winds, and geopotential height for the outermost domain. The SST data in WRF downscaling simulations are from the radiative surface temperature of CESM data. Bias correction is applied to radiative surface temperature based on skin temperature from NARR in this study.

The periods of 2003–2012 and 2046–2055 were selected to represent a present and a future decadal period in this study. North American Regional Reanalysis data (NARR; Mesinger et al. 2006), which covers North America with a 32 km horizontal resolution and 29 vertical levels, from the 2003–2012 period was used as a benchmark to estimate the biases of the CESM simulations for the present decade. Both the climatological means and the interannual variations of the CESM data are adjusted based on NARR data for 2003–2012 (Xu and Yang 2012; Zhao et al. 2020). The interannual variations are adjusted by scaling the variations of the CESM data to those of the NARR data for the same calendar month. This bias correction method was selected for this study because it has been shown to be superior to the traditional linear bias correction method in improving the probability distributions of meteorological variables and capturing extreme weather events from the downscaled model results, which is a major focus of this study (Xu and Yang 2012; Zhao et al. 2020). Bias correction was applied to 3-dimensional (3D) air temperatures, zonal and meridional

winds, water vapor mixing ratios, and geopotential heights, as well as air temperatures and relative humidities at two meters above ground level (AGL) and surface skin temperature. The bias correction is tuned for each calendar month and applied on a 6-hourly basis. Zhao et al. (2020) demonstrates the time-invariance of the biases of the CESM data relative to NARR data by applying the bias correction coefficients to two validation periods (i.e. 1980–1989 and 1990–1999). Thus, these derived bias correction coefficients are applied to adjust the biases of the CESM data for both the current and future simulation periods in this study.

3 Evaluation of the dynamical downscaling results with bias correction method

The WRF model performance driven by CESM data with (D_BCCESM) and without (D_OCESM) bias correction is evaluated against the WRF simulation driven by NARR reanalysis (D_NARR) using the 10-year averaged values from the present climate (i.e., 2003–2012). Note that

the model results from the WRF simulations with 12×12 km^2 horizontal grid size are used in this section because D_OCESM is conducted using only the outer two WRF domains with 36×36 and 12×12 km^2 resolutions. The analyses are focused on the nine geographical sub-regions over California, the names and abbreviations of these nine sub-regions are listed in Table S1, while the locations of these sub-regions can be found in Fig. 2b in Zhao et al. (2020). Compared to D_NARR, D_OCESM simulates warmer 2-m temperature (T2) over the coastal area, Pacific Ocean off the California coast, and mountain ranges surrounding the CV but colder T2 over MD (Fig. 1a). Driven by bias-corrected CESM data (D_BCCESM), both the positive and negative T2 differences are reduced considerably over California (Fig. 1b). Figure S1a and Table S2 show that regional mean T2 differences between D_BCCESM and D_NARR are smaller compared to those between D_OCESM and D_NARR for 8 out of 9 sub-regions, within which the differences are reduced by over 50% for 6 sub-regions (i.e. GBV, SJV, SAC, BA, SC and SCC). Due to the co-existence of both positive and negative differences between D_OCESM
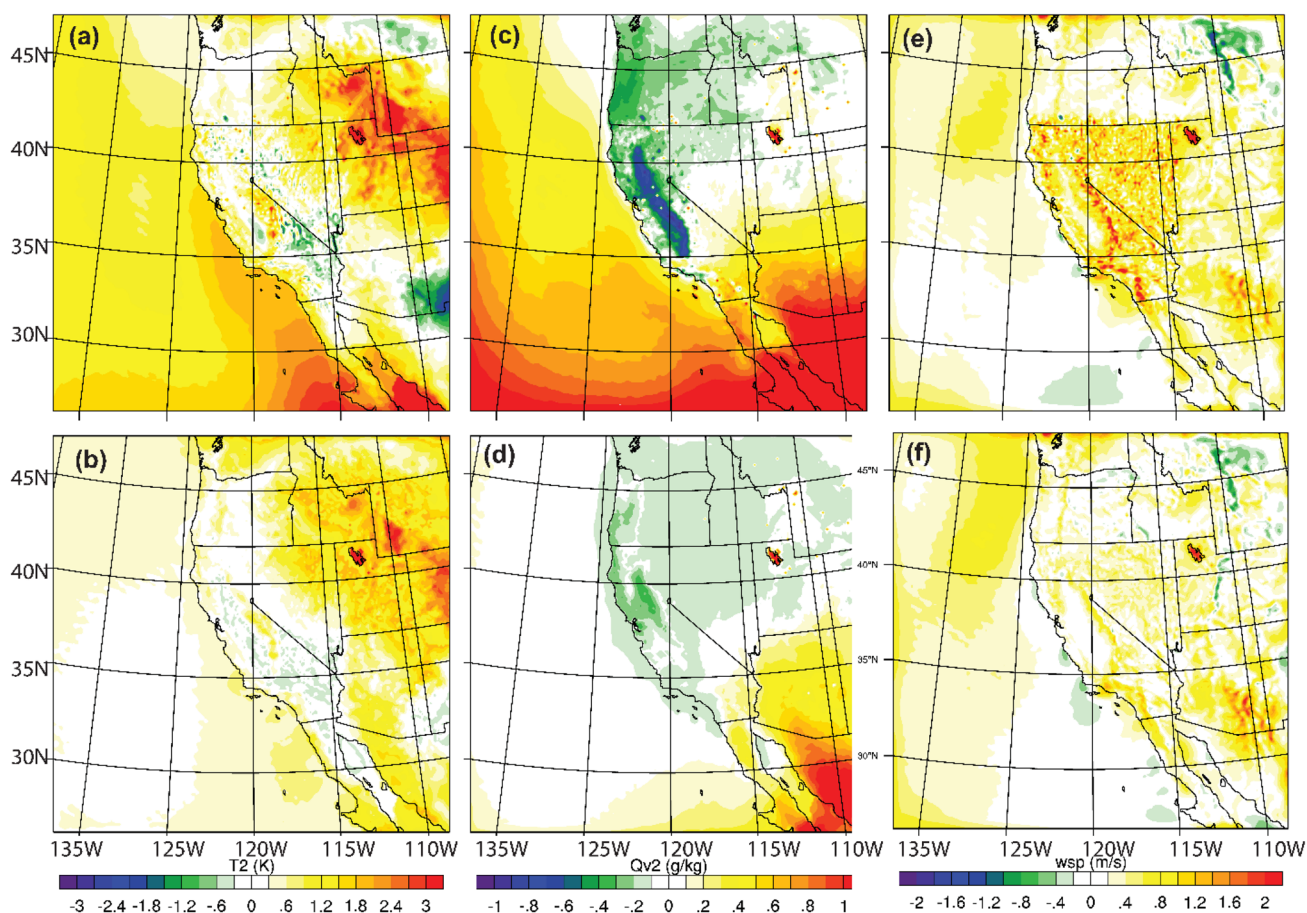

Fig. 1 Differences of wintertime mean T2 (in K; left), Qv2 (in g/kg; middle), and wsp10 (in m/s; right) from D_OCESM (top) and D_BCCESM (bottom) relative to D_NARR

and D_NARR, the spatial variation of T2 differences over GBV is much greater than those over other sub-regions (Fig. S1a). Figures 1 and S1a illustrate substantially smaller spatial variations of T2 differences in most sub-regions from D_BCCESM than those from D_OCESM compared to D_NARR, indicating better resemblance of simulated spatial patterns of T2 between D_BCCESM and D_NARR.

Compared to D_NARR, D_OCESM simulates lower Qv2 over northern California, especially over the CV, and higher Qv2 over the southern California and off the coast of California (Fig. 1c). These discrepancies, as well as disagreements in Qv2 for other areas within the domain, are reduced substantially when using bias-corrected CESM data (Fig. 1d). Regional mean Qv2 differences between D_BCCESM and D_NARR are smaller than those between D_OCESM and D_NARR for 7 out of 9 sub-regions (Fig. S1b and Table S2). Figure S1b again shows substantially smaller spatial variations of differences in Qv2 from D_BCCESM than from D_OCESM compared to D_NARR, suggesting an overall better agreement of Qv2 spatial patterns between D_BCCESM and D_NARR than between D_OCESM and D_NARR.

The 10-m wind speeds (wsp10) in D_OCESM are overestimated compared to those in D_NARR, especially over the mountain ranges surrounding the CV (Figs. 1e and S1c). Driven by bias-corrected CESM data (i.e., D_BCCESM), the wsp10 overestimation over California in D_OCESM is reduced remarkably over California (Fig. 1f). Figure S1c and Table S2 show that both the regional mean and spatial variation of wsp10 differences from D_OCESM are reduced considerably for all 9 sub-regions as a result of the bias correction of the CESM data.

In addition, Global Precipitation Climatology Centre (GPCC) monthly precipitation dataset (https://www.dwd.de/EN/ourservices/gpcc/gpcc.html) is used to assess the simulated monthly total precipitation from D_BCCESM and D_OCESM for wintertime. The GPCC V7 is used here, which provides monthly values from 1901 through 2013 based on quality-controlled data from 67,200 stations world-wide. The GPCC V7 dataset has a spatial resolution of $0.5° \times 0.5°$. The 10-year mean monthly total precipitation amounts averaged over the winter months from D_OCESM, D_BCCESM and GPCC data are shown in Fig. 2. GPCC data show higher precipitation (up to 200 mm/month) over northern California, Sierra Nevada Mountain Ranges, as well as western part of Oregon and Washington states (Fig. 2d) than other areas within the model domain. The spatial patterns are reproduced by D_OCESM (Fig. 2a) and D_BCCESM (Fig. 2b). However, the magnitude of the precipitation is over-estimated by both D_OCESM and D_BCCESM with that D_BCCESM performs better than D_OCESM for most of the domain. Figure 2c illustrates that D_BCCESM produces lower precipitation than D_OCESM for most of the model domain, especially over the aforementioned regions

with higher GPCC precipitation (i.e. northern California, Sierra Nevada Mountain Ranges) in which the precipitation estimated by D_BCCESM can be lower up to 60 mm/month compared to D_OCESM. In other words, the precipitation overestimation from D_OCESM relative to GPCC data is reduced considerably as a result of the bias correction of the CESM data. In summary, as shown in Fig. 2, D_BCCESM has better agreement with GPCC data in the spatial pattern and magnitude of the monthly total precipitation than does D_OCESM. Note that 3 domains are used for D_BCCESM, whereas only the outer 2 domains are used for D_OCESM. Figure 2a–c show the modeling results from the 2nd domain with a 12-km resolution, while the box inside Fig. 2b, c is due to the feedback from the 3rd model domain (a child domain), which has a 4-km horizontal resolution.

Simulated upper-air geopotential height (GPH) and temperature fields are evaluated against the D_NARR data. Compared to D_NARR, smaller differences in GPH are obtained after using the bias-corrected CESM data (i.e., D_BCCESM versus D_OCESM), and the GPH differences between D_BCCESM and D_NARR are almost negligible over California at both 500 hPa and 850 hPa (Fig. S2). Compared to D_NARR, differences in upper-air temperatures from D_OCESM are also reduced considerably over most of the domain at both 500 hPa and 850 hPa as a result of the bias correction (Fig. S3).

WRF downscaled results are also compared to surface observations from the Federal Aviation Administration (FAA) and the U.S. Environmental Protection Agency (EPA) Aerometric Information Retrieval System (AIRS) over SJV and SC to further evaluate model performance with and without CESM bias correction. A total of 35 (30) stations for T2 over SJV (SC), 18 (25) stations for RH2 over SJV (SC), and 36 (43) stations for wsp10 over SJV (SC) are used for the comparison. Figure S4 shows the modeled winter mean biases of T2, Qv2 and wsp10 over SJV and SC averaged over all stations within each sub-region, where observations are available. WRF simulated biases for T2 are reduced from 0.42 K (0.23 K) to − 0.29 K (− 0.14 K) over SJV (SC) as a result of the bias correction, while RH2 biases are reduced from − 5.2% (− 6.4%) to 0.9% (− 5.3%) for SJV (SC). Wind speed biases are also reduced slightly after bias correction of the CESM data.

4 Climate projections for wintertime variables over California

In this section, the projected future changes in meteorological variables that are important to winter PM formation and buildup over California are investigated. Model outputs from the innermost domain with a horizontal resolution of 4×4 km^2 are used in this section, as well as in the following
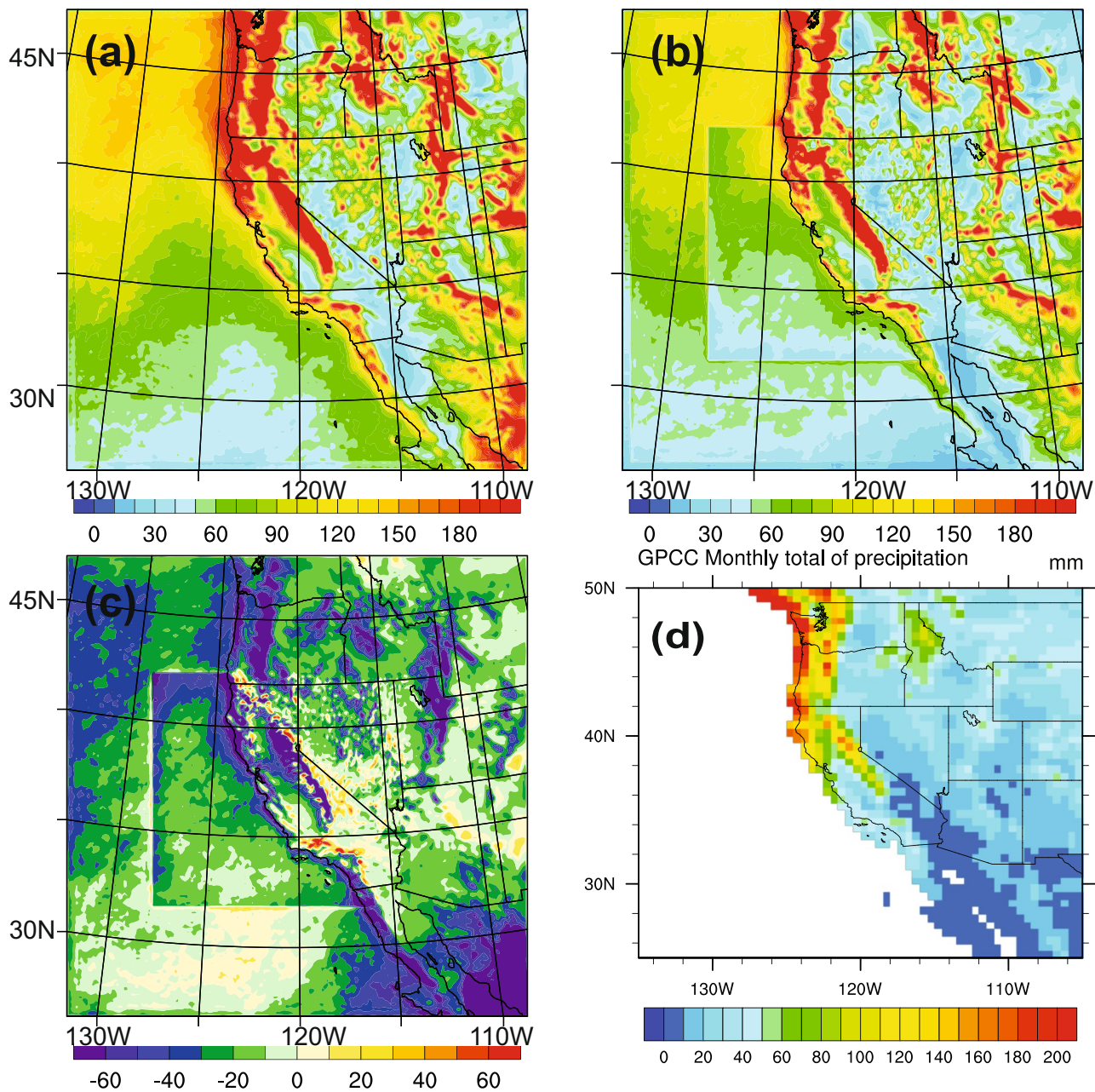
Fig. 2 Winter mean monthly total precipitation (in mm) averaged for 2003–2012 from the following: **a** D_OCESM, **b** D_BCCESM, and **d** GPCC. The difference in winter mean monthly total precipitation between D_BCCESM and D_OCESM (i.e. **b–a**) is shown in **c**

sections. Figure 3 shows future changes in T2, Qv2, PBLH and wsp10 averaged over the winter months (e.g., December to March). The projected future changes in the variables of interest are considered statistically significant if the p-value is smaller than 0.05 (95% confidence; Zhao et al. 2020). The results show that the projected future increase in daily mean T2 averaged over the winter months is up to 2 K over California, and the greatest increase is predicted to occur over the mountain ranges surrounding the CV (Fig. 3a). The regional daily mean T2 increases are over 1 K for all 9

sub-regions, within which the increases over 1.5 K are GBV, SCC and SJV (Table 1). The greater increase in nighttime temperatures compared to daytime temperatures results in a smaller wintertime daily temperature range (DTR), which is consistent with projected changes during summertime (Zhao et al. 2020; Fig. S5). A projected future increase in Qv2 is observed for the entire domain, and a greater increase in Qv2 (up to 1 g/kg) occurs in the CV and along the coast of California than that in inland regions (Fig. 3b and Table 1). Figure 3a, b and Table 1 show that the projected increases
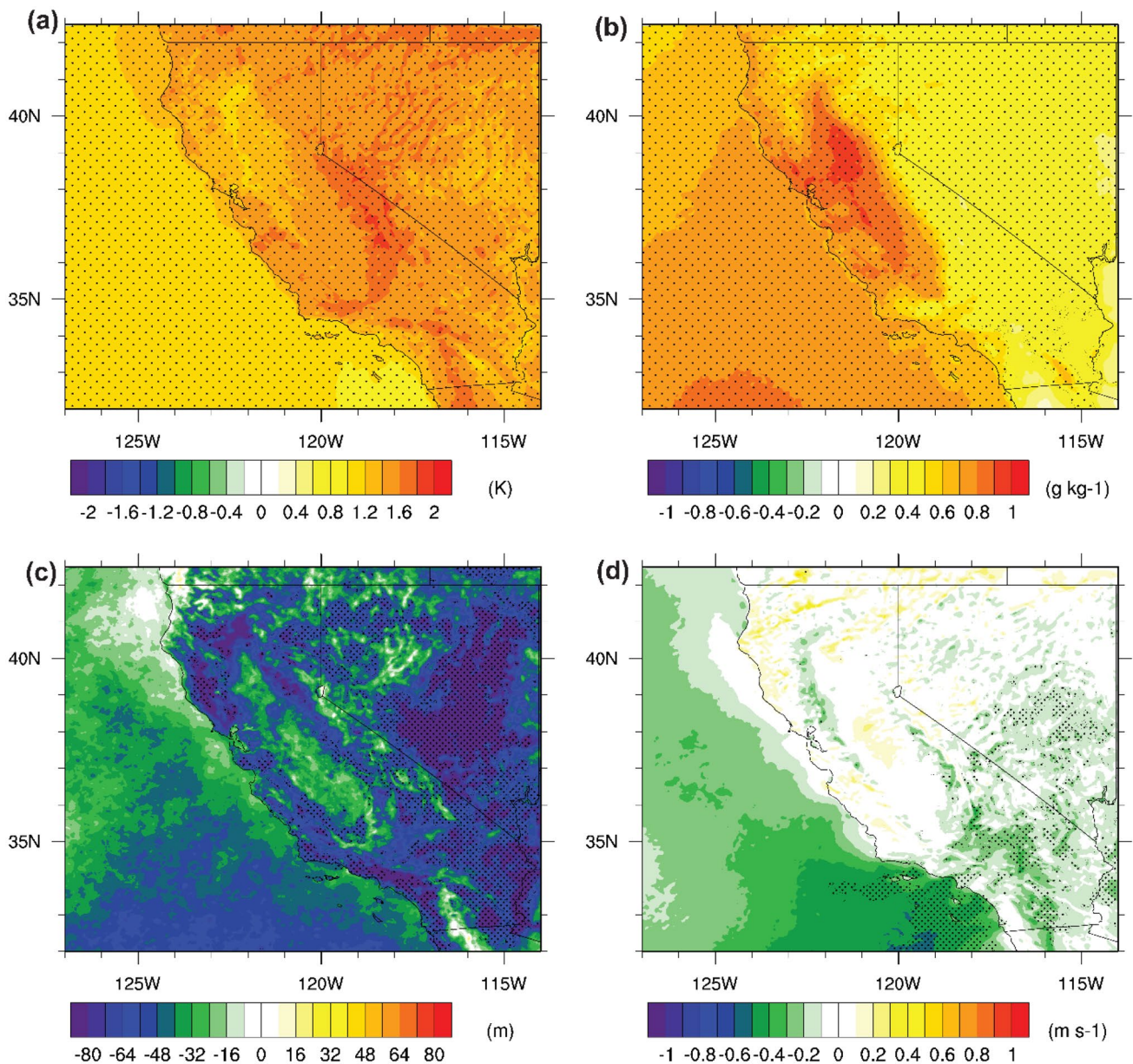
Fig. 3 Future changes in: **a** daily mean T2 (K), **b** daily mean Qv2 (g/kg), **c** PBLH (m) at 2 pm PST, and **d** daily mean wsp10 (m/s); averaged over the winter months. Regions with 95% confidence level ($p < 0.05$) of the future changes in these variables are shaded with dots

Table 1 Future changes of wintertime daily mean 2-m T, 2-m Qv; daily maximum PBLH, and daily mean 10-m wind speed, averaged for the nine geophysical sub-regions

	BA	GBV	MC	MD	NC	SAC	SCC	SC	SJV
T2 (K)	**1.38**	**1.62**	**1.49**	**1.49**	**1.4**	**1.28**	**1.52**	**1.43**	**1.51**
Qv2 (g/kg)	**0.84**	**0.39**	**0.65**	**0.40**	**0.71**	**0.78**	**0.65**	**0.51**	**0.70**
PBLH_max (m)	− 59.5	− 48.2	− 52.3	− 64	− 53.5	− 56.3	− 61.8	− 68.3	− 41
wsp10 (m/s)	− 0.04	− 0.08	**0.01**	− 0.18	**0.07**	− 0.05	− 0.02	− 0.16	− 0.03

Positive changes are highlighted with boldface

in daily mean T2 and Qv2 over California are greater for wintertime than for summertime (Zhao et al. 2020), and the projected increases in these two variables for wintertime

are statistically significant for almost all of California and the Pacific Ocean off the coast of California. Different from summertime, a projected future decrease in daily maximum

PBLH (PBLH_max) during winter is observed over the entire domain, and this projected decrease is statistically significant over most of the coastal regions and the arid MD, as well as part of the mountain ranges (Fig. 3c). The future decrease in PBLH_max is greater over the coastal areas (SC, SCC and BA) and the arid region (MD) than over the rest of California (Fig. 3c and Table 1). The percentage of future decrease in PBLH_max is projected to be more than 10% for BA and mountain ranges in northern California, (i.e. Northern Coast Ranges and Klamath Mountains; figures not shown). The future changes in wsp10, which range from − 0.5 to 0.5 m/s over California, are less obvious than the other three meteorological variables over California. The projected wsp10 changes are only statistically significant for some areas over southern California, where the wsp10 is projected to decrease by up to 0.5 m/s (Fig. 3d). The projected decreases in PBLH_max and wsp10 are conducive to the accumulation of winter PM, which indicates a potential exacerbation of existing winter PM issues over these regions in the future. Please note that the result presented in this study is based on a single future climate realization. Thus, the more pronounced changes of T2, Qv2 and PBLH_max in future wintertime than in future summertime obtained in this study may not represent the consensus from other GCMs (Deser et al. 2016).

The projected change in the probability distribution of state-averaged surface temperature, which is calculated by averaging over the model grids within California, is also explored. The probability distribution of daily mean (T_{mean}), daily minimum (T_{min}) and daily maximum (T_{max}) of the state-averaged T2 for the current and future decades are illustrated in Fig. 4. Compared to the present decade, the means of the T_{mean}, T_{min}, and T_{max} are shifted to warmer temperatures by 1.43 K, 1.61 K and 1.20 K in the future decade, respectively. A tendency towards more negative skewness in the future climate is observed for T_{min} and T_{mean} (Fig. 4). This can be, at least partially, due to the fact that cold anomaly of the future climate from its mean keeps a similar distribution as the current climate but shifts to a warmer temperature; however, the warm anomaly of the future climate from its mean is skewed toward the warmer temperature with a smaller range. The projected future shifts of the 5th percentiles for these three parameters are remarkably greater than those of the mean and the 95th percentiles. For instance, the shift for the 5th percentile of T_{min} (2.20 K) is approximately 37% greater than that for the mean (1.61 K) and three times greater than that for the 95th percentile (0.55 K). As shown in Fig. 4, a larger shift of the left tail than the right tail towards the hotter temperature of the distribution is observed for all three parameters. As a result, a future reduction in the variance is observed for all three parameters, implying a narrower probability distribution for these parameters in
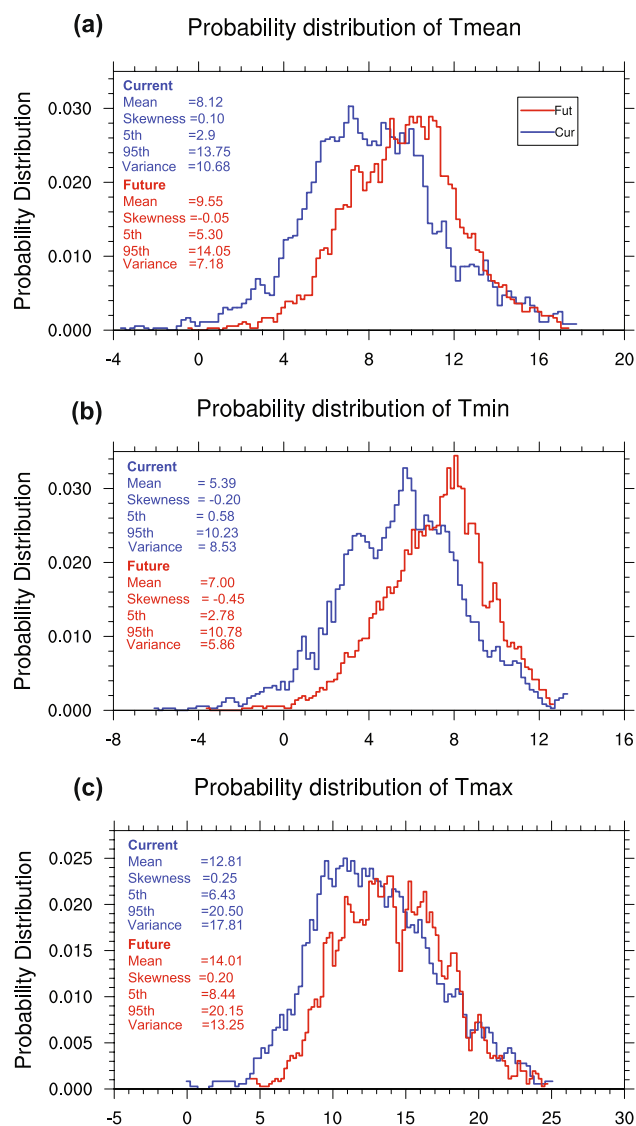

Fig. 4 Probability distribution of state-mean for: **a** daily mean, **b** daily minimum, and **c** daily maximum T2; for current (2003–2012 in blue) and future (2046–2055 in red); with 100 bins. Statistics (mean, skewness, 5th and 95th percentiles, and variance) for each dataset are shown in each panel

the future decade. Figure 4 also illustrates greater climate change impact on T_{min} than T_{max}. The considerable shift of the probability distribution of the state mean surface temperature to warmer temperature for the future simulation period shown in Fig. 4, especially T_{min}, indicates that more snow will melt during winter and early spring and less snowpack over Sierra Nevada will be available for the water supply for the following late spring and summer in California in the future, which is discussed next. This can lead to an increase in the risk of drought and potentially catastrophic wildfires.

5 Precipitation analysis

As described in the introduction, wintertime precipitation and the resultant snowpack over the Sierra Nevada are vital for water supplies in California, and thus it is important to investigate the projected future changes in wintertime precipitation over California. Precipitation is in the form of rain, snow and graupel in the WSM6 microphysics, which is used in the WRF downscaling simulations in this study. The winter-mean daily precipitation (Pr_daily_tot) in Fig. 5 is the sum of precipitation in all

three forms. Figure 5a, b demonstrate that the maximum Pr_daily_tot occurs over the mountain ranges for both the current and future decades and Pr_daily_tot is generally higher over northern California than it is over southern California. Figure 5c, d illustrate a future increase in Pr_daily_tot over northern California by up to 50% compared to the current decade; whereas, an up to 40% future reduction in Pr_daily_tot is expected over southern California. The projected precipitation changes are statistically significant over most of northern California and part of GBV (Fig. 5c). The relatively wet (dry) northern (southern) California is projected to become wetter (drier) by
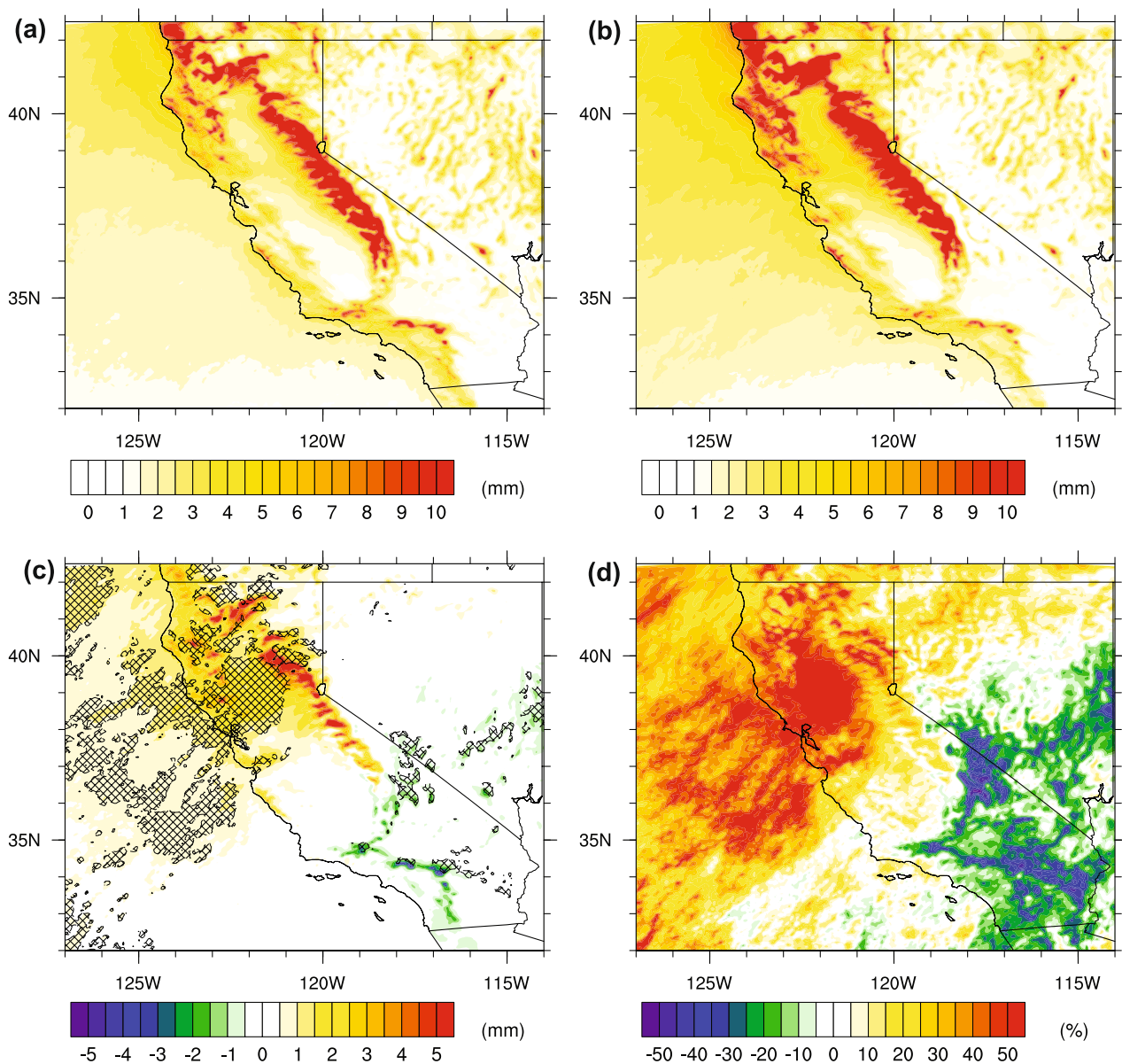

Fig. 5 Pr_daily_tot (in mm) for the following: **a** current decade, **b** future decade (in mm), **c** future changes in Pr_daily_tot (in mm) with respect to the current climate, and **d** percentage of future changes (in %) in Pr_daily_tot; relative to the current decade. Regions with 95% confidence level ($p < 0.05$) of the future changes in Pr_daily_tot are shaded with cross-hatching in **c**

the 2050s. Similar findings are reported in previous studies (Swain et al. 2014; Ullrich et al. 2018). Meehl et al. (2007) reported that the large-scale climate change signals associated with global warming tend to result in a reduction in precipitation over the subtropics and an increase in precipitation at mid-to-high latitudes. California is located in the region between these opposing tendencies, which may explain some of the differences in the direction of the future changes in precipitation patterns for northern and southern California shown in Fig. 5. This also implies that since California lies between the mid-to-high latitudes and the subtropics, future projections of precipitation are likely more uncertain. Five sub-regions in northern California are projected to receive more precipitation in the future decade (Fig. 6). The regional mean Pr_daily_tot values are predicted to increase by 2.6 mm, 2.5 mm, 2.2 mm, 1.6 mm, and 0.4 mm for MC, NC, SAC, BA and SJV, respectively, which correspond to percent increases of 28.8%, 35.8%, 45.8%, 50.2% and 10.1%, respectively. In contrast, four sub-regions over southern California are projected to receive less precipitation in the future decade (Fig. 6). The regional means of Pr_daily_tot are projected to decease by 0.73 mm, 0.06 mm, 0.02 mm and 0.33 mm for SC, SCC, GBV and MD, respectively. MD, the driest region in California, is projected to experience the largest future percent decrease of 22.5% in winter mean daily precipitation.

As stated in the introduction, wintertime snowpack at high altitudes is critical for California's water supply. Future changes in winter-mean daily precipitation in solid form (i.e. snow + graupel; Pr_daily_solid) as well as the snow_to_precipitation ratio, which is calculated as the ratio of Pr_daily_solid to Pr_daily_tot, are investigated. Figure 7a, c depict that most of the solid form precipitation is received over

the mountain ranges to the east and north sides of the CV, especially the Sierra Nevada, where Pr_daily_solid is up to 5 mm and the snow_to_precipitation ratio is up to 0.5. Figure 7b shows a reduction in Pr_daily_solid over the western side of the Sierra Nevada and the mountain ranges to the south of the CV, where the elevations range between 500 to 2000 m, and an increase (up to 2.5 mm) in Pr_daily_solid over the eastern side of the Sierra Nevada, where the elevations are over 2000 m. The opposite signs of future changes in Pr_daily_tot (Fig. 5c) and Pr_daily_solid (Fig. 7b) over the western side of the Sierra Nevada suggest that more wintertime precipitation will be received in liquid form over this region by the 2050s. The underlining reason for this phenomenon is that the significant warming (up to 2 K) over the mountain ranges in California (Figs. 3a and S5) may lead to longer periods with temperatures above the freezing point in areas where the elevation is lower than the eastern side of the Sierra Nevada. The significance test results in Fig. 7b illustrate that the reduction in Pr_daily_solid over the western side of the Sierra Nevada and the mountain range to the south of the CV is statistically significant at the 95% confidence level. A lower than 95% confidence level for the increase of Pr_daily_solid over the eastern side of the Sierra Nevada can be attributed to the relatively large inter-annual variations in snow received over this region. With respect to the snow_to_precipitation ratio, a future reduction is observed for most regions where the ratio is greater than zero (Fig. 7c), except for the eastern side of the Sierra Nevada where the elevation is over 2000 m and the future change in snow_to_precipitation ratio is close to zero (Fig. 7d). This indicates that the increase in Pr_daily_solid (Fig. 7b) is proportional to the increase in Pr_daily_tot (Fig. 5c) over the eastern side of the Sierra Nevada; whereas, a smaller percentage of Pr_daily_tot would be received in solid form over the mountain areas with elevation less than 2000 m in the future. This may lead to substantial changes in the snowpack distribution over the Sierra Nevada, affecting the state's water supply, by the 2050s.

Three-day accumulation of precipitation is an important indicator of the potential for flooding, because it normally takes a few days for soil to saturate (Das et al. 2011; Pierce et al. 2013). The cumulative distribution functions (CDF) of the area-averaged 3-day mean precipitation (precip_3day) for the nine sub-regions for the present and future decades are shown in Fig. 8. Four sub-regions (MC, NC, SAC and BA), all located in northern California, show a shift to a higher likelihood of greater precip_3day at all probability levels. The CDFs for these four sub-regions show greater increases at the higher percentile values and smaller changes below the median. For instance, the CDF of precip_3day for NC suggests that the chance of precip_3day greater than 20 mm over this region would increase from 10% for the present decade to 20% for the future decade. Figure 8 suggests
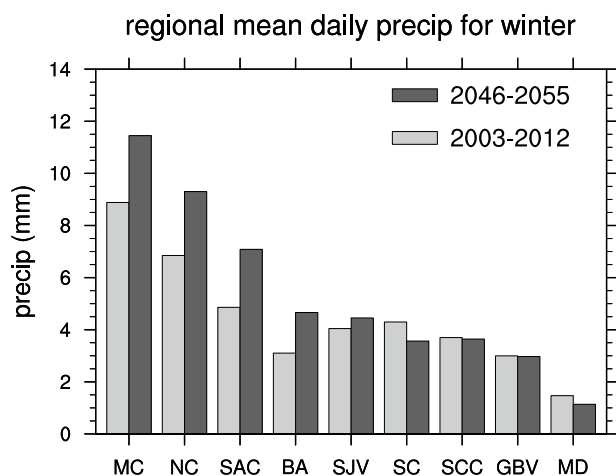

Fig. 6 Regional mean daily precipitation (mm) for the nine sub-regions averaged for the winter months for the current and future decade
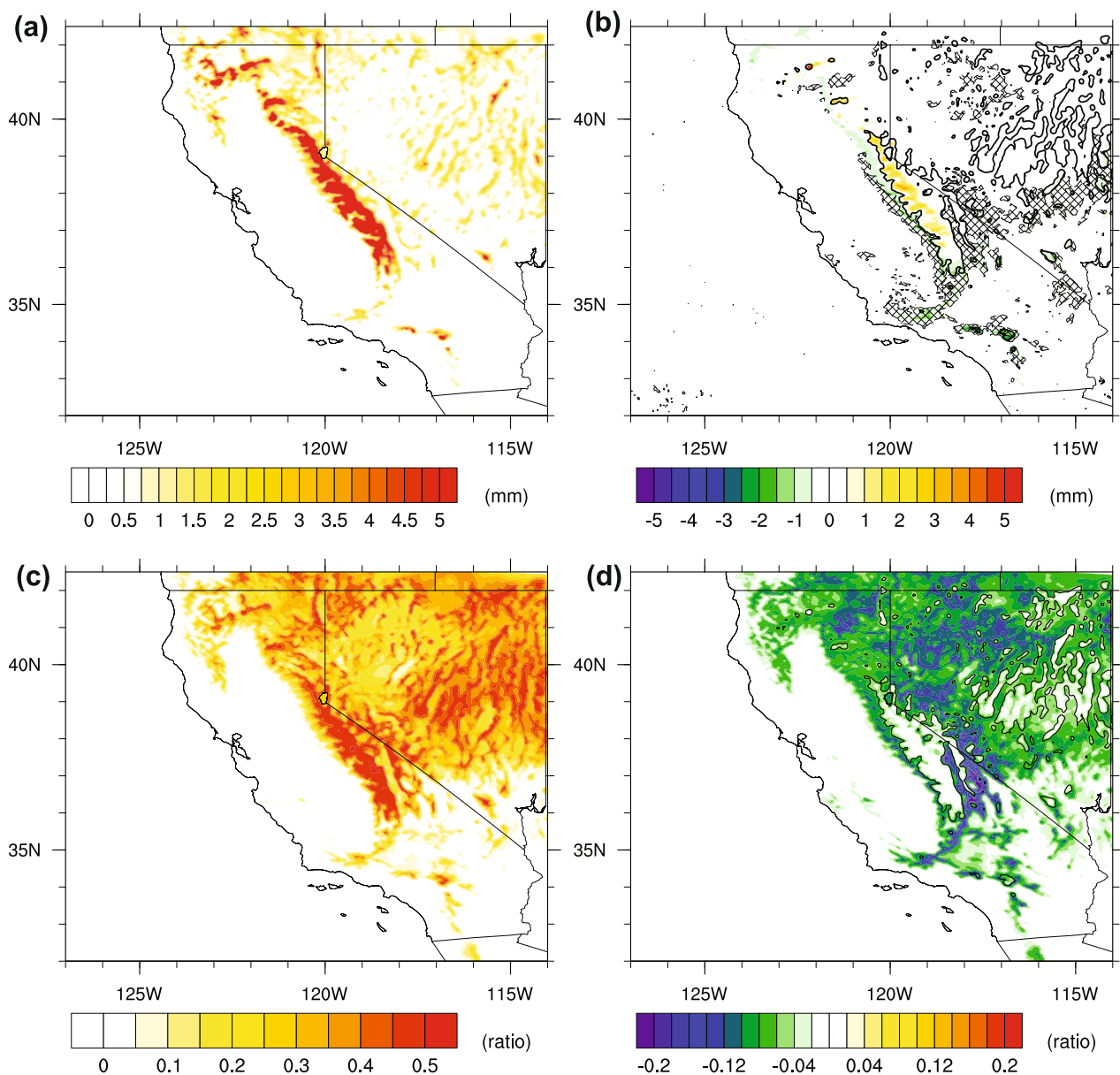
Fig. 7 Panels appear as follows: **a** Pr_daily_solid (mm) for the current decade, **b** future changes in Pr_daily_solid (mm), **c** snow_to_precipitation ratio for the current decade, and **d** future changes in snow_to_precipitation ratio. Solid black contours in **b** and **d** represent terrain height of 2000 m. Regions with 95% confidence level (p < 0.05) of the future changes in Pr_daily_solid are shaded with cross-hatching in **b**

that the future increase of precipitation for the sub-regions over northern California (Figs. 5 and 6) is attributed more to the increase in the frequency of wet extremes than the light precipitation events. An opposite CDF pattern is found for SJV. The future increase of 10.1% in winter precipitation over this region (Fig. 6) is likely attributed to more precipitation events/days with a smaller intensity. The future changes in CDF for SCC and GBV show a decrease at lower precip_3day values and an increase at higher precip_3day values, suggesting that there would be more precipitation events with smaller intensity and fewer precipitation

extremes over these two regions. The opposite trends at the two ends of the CDF plots for SCC and GBV (Fig. 8) result in a small future change in the regional mean precipitation amounts over these two regions (Fig. 6; − 1.5% and − 0.8% for SCC and GBV, respectively). The CDFs of precip_3day for SC and MD show a shift to a higher likelihood of smaller precip_3day at almost all probability levels with greater changes at the higher percentile values, indicating fewer wet extremes over these two regions in the future.

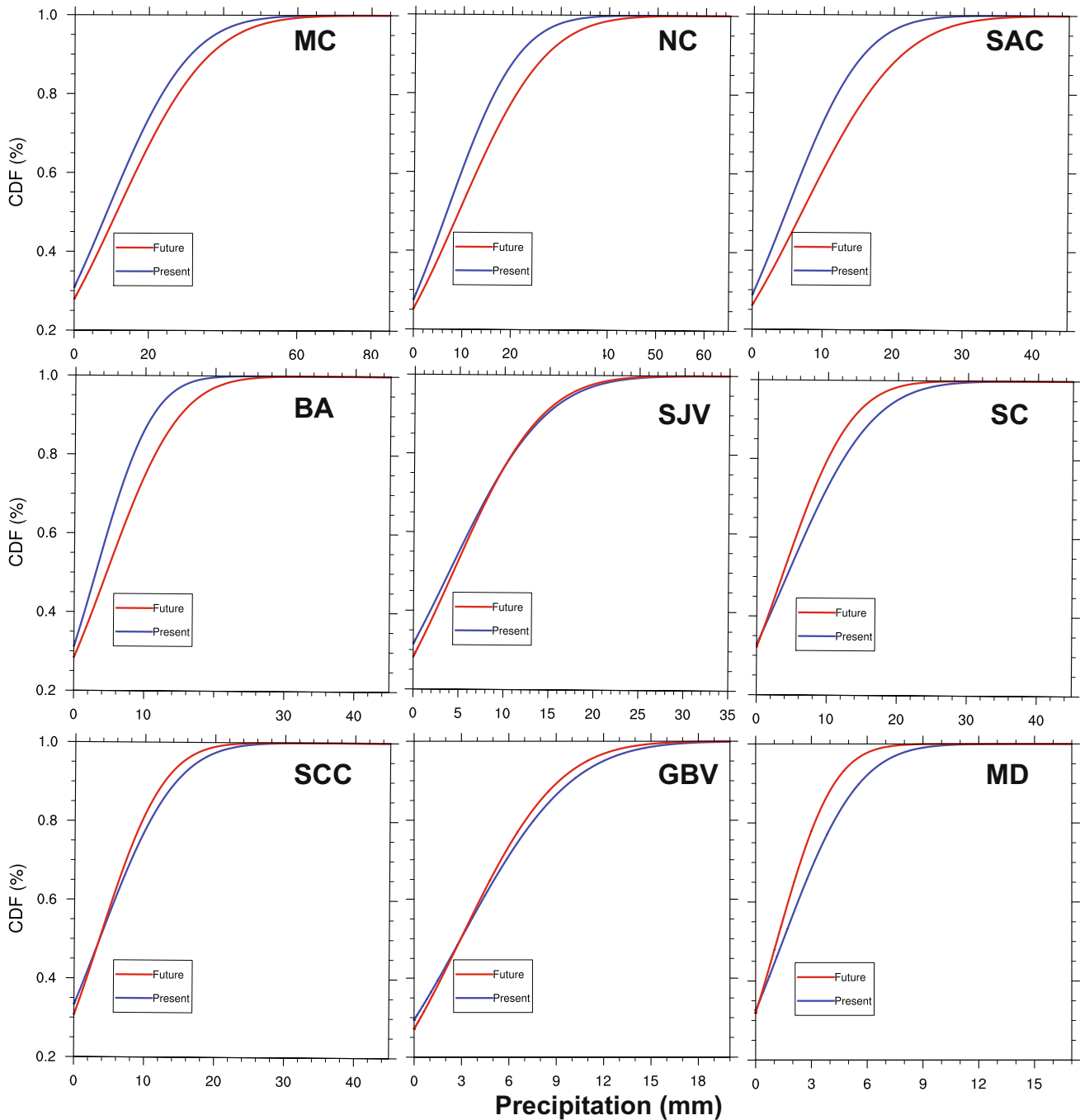The CDF for precip_3day in Fig. 8 suggests that the future increase in precipitation over the northern California

Fig. 8 Cumulative distribution functions (CDFs) of area-averaged 3-day mean precipitation (in mm) for the nine sub-regions for the present (blue line) and the future (red line) decades. The y axis is the probability (0–1) of experiencing the indicated average 3-day precipitation rate (mm/day) or lower

is primarily due to the future increase in the occurrences of wet extremes. Previous observational and modeling studies show that wet extremes and flooding events over California are often associated with landfalling ARs over the west coast of the U.S. (Neiman et al. 2008a, b; Leung and Qian 2009; Dettinger 2011). Guan et al. (2012) show that landfalling ARs contribute up to 30–40% of total wintertime snow accumulation in the Sierra Nevada. Previous studies have reported future increase in AR activities and intensities along the west coast of the U.S. (Dettinger 2011; Gao

et al. 2015; Warner et al. 2015), largely due to the increase in the water vapor holding capacity of the atmosphere as the climate warms (Held and Soden 2006). The climate change impact on ARs and the correlation between the future changes in ARs and precipitation over California are explored here. Daily low-level integrated water vapor transport (IVT) is commonly used for AR detection along the U.S. west coast because studies have demonstrated a close relationship between offshore IVT and the orographic rainfall over California's coast (Ralph et al. 2006; Neiman et al. 2008b). Dettinger (2011) and Warner et al. (2015) used IVT at locations off the west coast calculated from GCM data to examine changes in ARs affecting the U.S. west coast. Following Dettinger (2011) and Warner et al. (2015), this study identifies 15 CESM grid points off the U.S. west coast (Fig. 9 and Table 2), and calculates IVT values at these locations based on the bias-corrected wintertime CESM results for the current and future decades. IVT is calculated by vertically integrating the moisture transport between 1000 and 500 hPa pressure levels as shown in the following formula (Gao et al. 2015; Lavers et al. 2012):

$$IVT = \sqrt{\left(\frac{1}{g}\int_{1000}^{500}\overline{q}\,\overline{U}\,dp\right)^2 + \left(\frac{1}{g}\int_{1000}^{500}\overline{q}\,\overline{V}\,dp\right)^2} \qquad (1)$$

where g is the gravitational acceleration (m s^{-2}), $\overline{q}$ is the mean layer specific humidity (kg kg^{-1}), U and V are the mean layer zonal and meridional winds (m s^{-1}), respectively, and dp is the pressure difference (hPa) of the layer between two levels. The IVT values at the 98th percentile calculated for each grid cell shown in Fig. 9 for the winter months of the current decade (IVT_98th_Cur) are shown in Table 2, and these values are used as thresholds for IVT analysis. The number of days in the winter months of the future decade surpassing IVT_98th_Cur (Days_fut), as well as the percentage increase in number of days surpassing IVT_98th_Cur compared to that of the current decade (Perc_incr), for each grid cell are also calculated and shown in Table 2. Table 2 shows that the IVT_98th_Cur generally decreases from north (point 1) to south (point 15). Except

Fig. 9 CESM grid cells used for IVT analysis
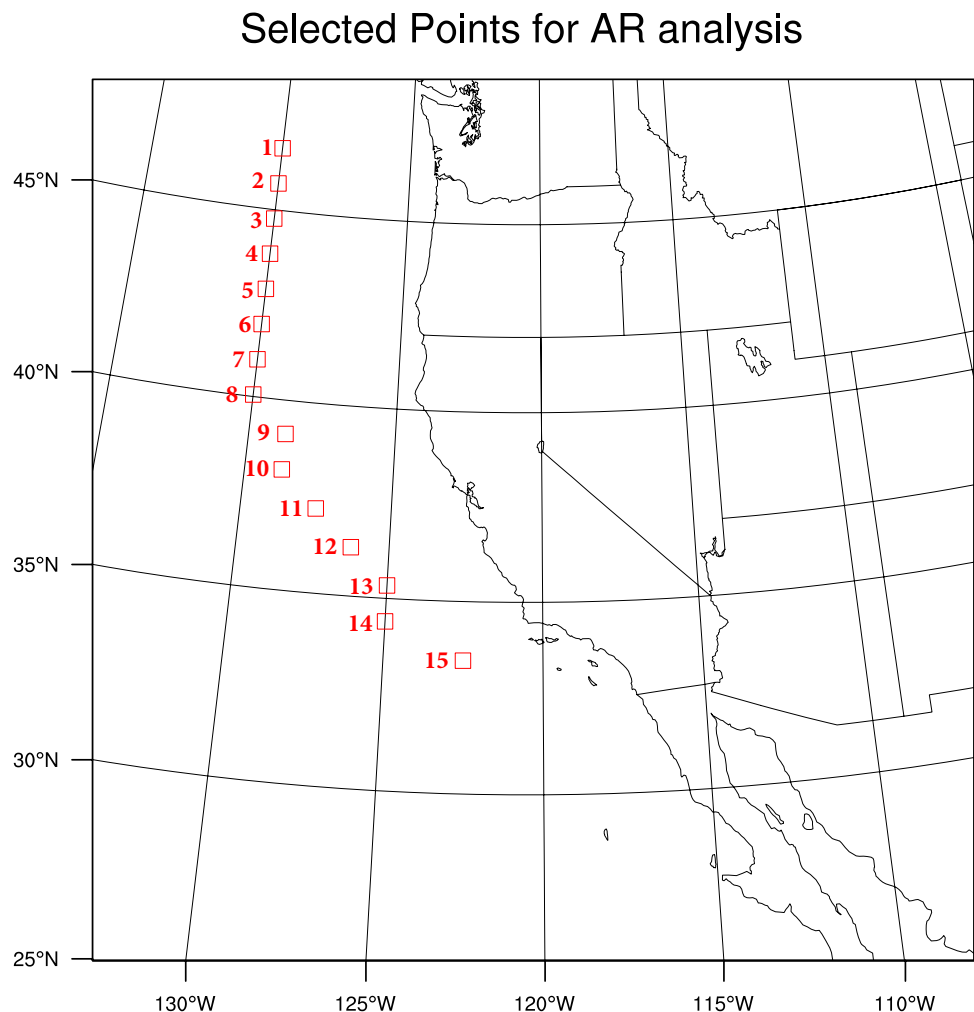

Selected Points for AR analysis

Table 2 IVT 98th percentile threshold for the current decade (IVT_98th_Cur), number of days surpassing the current threshold in the future decade (Days_Fut), and the percentage increase (Perc_incr) over the current decade in number of days surpassing the threshold for the future decade for the 15 CESM grid points shown in Fig. 9

| Grid points	Lat (°N)	IVT_98th_Cur (kg m^{-1} s^{-1})	Days_fut (days)	Perc_incr (%)
1	46.65	329.9	32	33
2	45.71	332.42	30	25
3	44.76	323.46	33	38
4	43.82	325.06	40	67
5	42.88	311.49	47	96
6	41.94	314.41	40	67
7	40.99	304.75	51	113
8	40.05	302.12	55	129
9	39.11	283.37	61	154
10	38.17	268.99	64	167
11	37.23	256.63	72	200
12	36.28	239.97	78	225
13	35.34	228.58	68	183
14	34.40	232.70	54	125
15	33.46	187.75	57	138

for point 15, IVT_98th_Cur values at all other 14 points are close to or greater than 250 kg m^{-1} s^{-1}, which is the IVT threshold value used to identify ARs in several previous studies (Gao et al. 2015; Cordeira et al. 2013; Rutz et al. 2014). Therefore, it is reasonable to use IVT_98th_Cur as an indicator of the activities of ARs approaching the U.S. west coast. Days_fut is greater than 24 days, which is the number of days with IVT greater than IVT_98th_Cur in the current decade, at all 15 points. Perc_incr ranges from 25 to 225% with the greatest increase between 35° and 40° N (points 9–13 in Fig. 9), mainly off the coast of northern and central California. Figure 10 illustrates the IVT values at the 98th percentile and winter mean for the current and future decade for the 15 points along the transect shown in Fig. 9,

respectively. Future increases are projected for both the 98th percentile and winter mean IVT values at all locations; however, the increase in the 98th percentile IVT is much more pronounced than that for the winter mean at all locations. A maximum future increase of 32% and 33% in the 98th percentile IVT are observed at grid point 9 (39.11° N) and 10 (38.17° N), respectively. The peak 98th percentile IVT values for the current and future decades are found at point 2 (45.71° N) and point 9 (39.11° N), respectively. Both Table 2 and Fig. 10 suggest that the peak of the ARs approaching the U.S. west coast during winter shifts southward from higher latitudes to the California coast in the future, especially between 35° to 40° N, which is consistent with the findings reported in previous studies (Gao et al. 2015; Warner et al. 2015). As stated previously, the projected future increases in precipitation over northern California are caused primarily by the increase in the number of days with extreme precipitation, which is likely attributed to the substantial future increase in the number of AR days and AR intensity between 35° to 40° N that make landfall in central and northern California (Polade et al. 2017; Gershunov et al. 2019).

6 Stagnation projection over SJV

Atmospheric stagnation is characterized by shallow PBLH, weak wind, no precipitation, and stable air conditions. SJV usually experiences the highest concentrations of winter PM in the U.S. (Chen et al. 2020), which is highly associated with atmospherically stagnant conditions over this region (Herner et al. 2005; 2006; Ham et al. 2010). In this study, the meteorological criteria defining stagnation in SJV is a combination of the widely used Air Stagnation Index (ASI), which uses daily precipitation, 10-m and 500-hPa wind speeds as thresholds (Wang and Angell 1999; Horton et al. 2012), and the meteorological criteria for regulating agricultural and prescribed burning in SJV, which is included in the Smoke Management Guidelines for Agricultural and

Fig. 10 98th percentile IVT (red) and winter mean IVT (blue) for the current (dashed line) and future (solid line) decade along the 15 grid-cell transect in Fig. 9
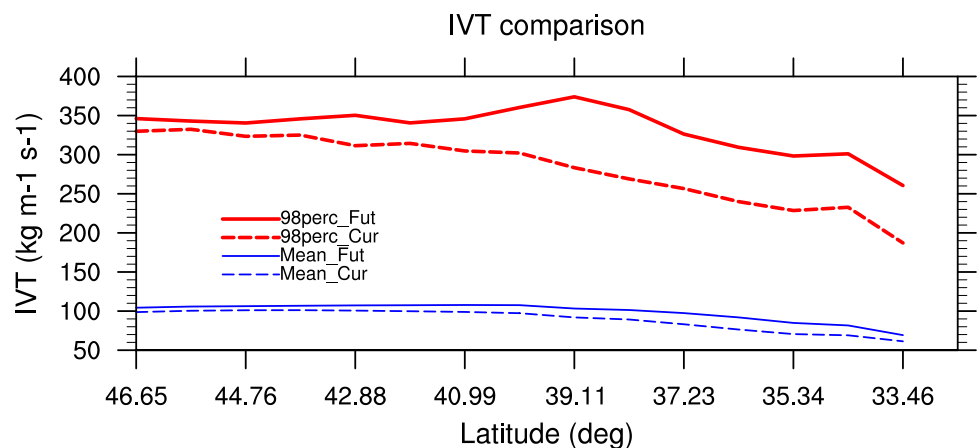
Prescribed Burning adopted by the California Air Resources Board (available at https://ww3.arb.ca.gov/smp/regs/revfi nregwtoc.pdf). These guidelines provide criteria for regulating agricultural and prescribed burning for each air basin in California. A WRF grid within SJV is considered stagnant when it meets the following four meteorological thresholds: (1) Daytime mean surface temperature is not warmer than temperatures at 3000 feet AGL by more than 11 F (the stability threshold); (2) daytime mean 10-m wind speed is less than 2 m/s (the near-surface wind threshold); (3) daytime mean wind speed at 3000 feet AGL is less than 4.5 m/s (the 3000 feet wind threshold); and (4) daily accumulated precipitation is less than 1 mm (the precipitation threshold). WRF results from 10 am to 2 pm during a day are averaged to calculate the daytime means for the variables used in the criteria. According to these criteria, the wintertime total numbers of stagnant days, averaged over SJV, during the 10-year historical and future periods are 202 and 214 days,

respectively, implying a 6% increase in winter stagnant days over SJV in the future. Figure 11e indicates that the increase of stagnant days mainly takes place over the eastern and central parts of SJV, where an increase up to 30 days in the total number of stagnant days is projected for the future decade when compared to the present decade. The future change in the occurrence of stagnation is the result of the combined responses of individual stagnation components in the criteria. Numbers of days meeting each of the four thresholds in the criteria are calculated to evaluate the influence of different factors on the overall increase in the occurrence of stagnation. A future increase in the number of days meeting the stability threshold is observed for almost the entire SJV region, and the increase is over 30 days for the majority of SJV (Fig. 11a). The number of days meeting the near-surface wind threshold decreases in the northeastern part of SJV, and increases for the rest of SJV for the future decade when compared to the current decade (Fig. 11b). In contrast,
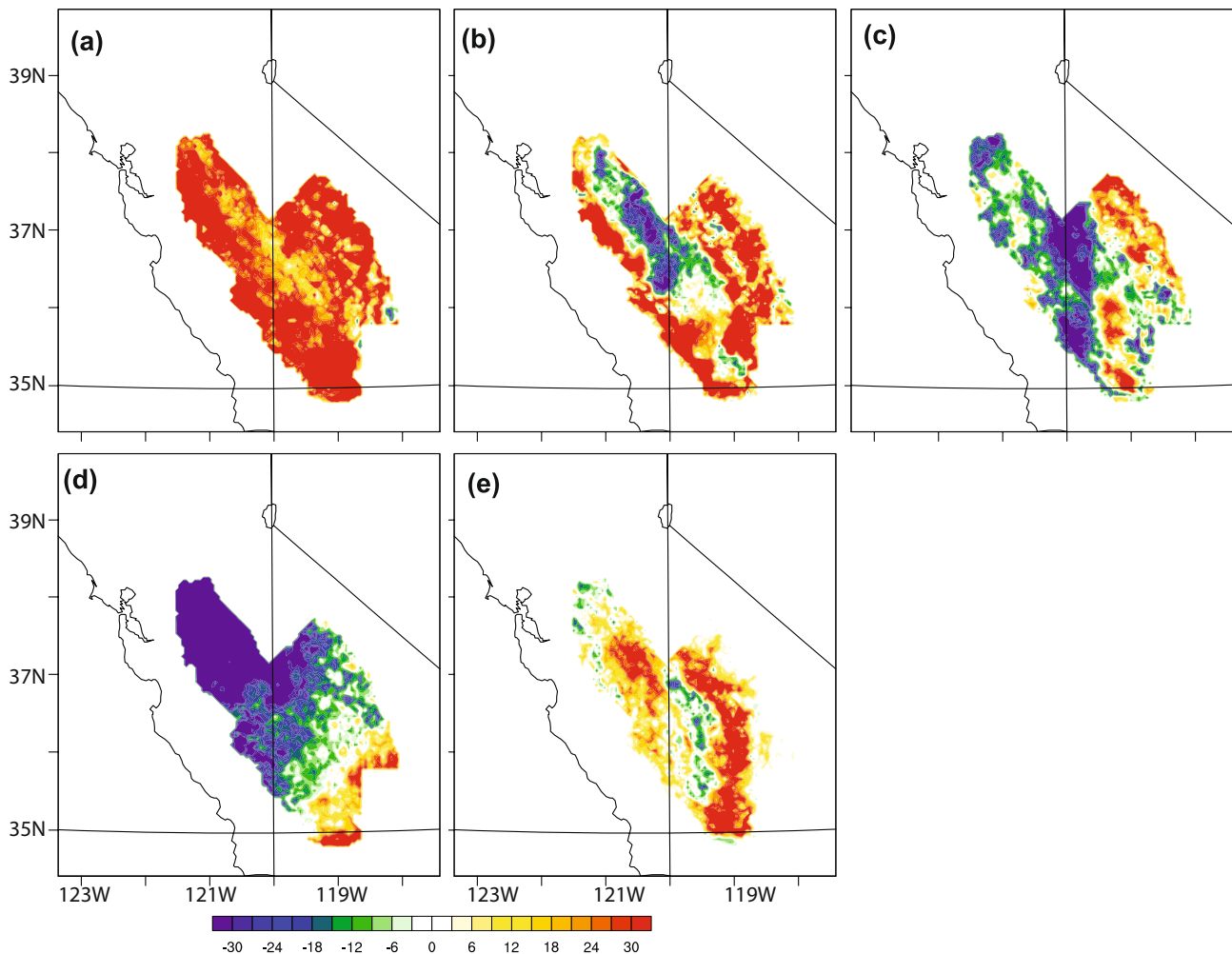

Fig. 11 Future changes in the total number of days in the entire decade meeting the thresholds for **a** stability **b** near-surface wind speed; **c** 3000 feet wind speed; **d** precipitation; and **e** meeting all the four thresholds over the SJV

the number of days meeting the 3000 feet wind threshold decreases (increases) for most of the western (eastern) part of SJV for the future decade when compared to the current decade (Fig. 11c). A future decrease (increase) in number of days meeting the precipitation threshold is observed for the northern (southern) part of SJV (Fig. 11d), which is consistent with the future change in precipitation over SJV shown in the previous section (Fig. 5c, d). Figure 11 illustrates that the projected future increase in the occurrence of the winter stagnation over SJV results from more frequent occurrences of days with more stable atmospheric flow and increases in near-surface and 3000 feet stagnant wind occurrences. Table 3 shows that averaged over SJV, there are 35 (20) more days meeting the stability (near-surface wind) threshold; whereas, there are 5 (20) fewer days meeting the 3000 feet wind (precipitation) threshold in the future simulation decade when compared to the current decade.

7 Conclusions

This study uses the WRF model to dynamically downscale CESM data from CMIP5 simulations with the RCP6.0 emission scenario to a 4×4 km^2 horizontal resolution over California for a present (2003–2012) and a future decade (2046–2055). The biases of the climatological mean and inter-annual variance of the CESM data are adjusted based on NARR reanalysis data between 2003 and 2012 prior to the downscaling process. The evaluation of the downscaled WRF results for the present decade and the analyses of future projections in meteorological variables and phenomena over California during summertime were presented in Zhao et al. (2020). This paper focuses on the evaluation of wintertime downscaled results and the investigation of projected future changes in wintertime meteorological variables, wintertime precipitation, and stagnation over California.

WRF downscaled results driven by bias corrected CESM data (D_BCCESM) for the present decade were compared with those driven by the original CESM data (D_OCESM) and by NARR reanalysis (D_NARR), Global Precipitation Climatology Centre (GPCC) monthly precipitation data, as well as surface observations. Comparisons were made on

variables of interest including 2-m temperature, 2-m water vapor mixing ratio, 10-m wind speed, precipitation, and geopotential height and temperature at 500 and 850 hPa. Comparison results show that as a result of the bias correction of the CESM data, the differences between D_BCCESM and D_NARR are substantially smaller than those between D_OCESM and D_NARR for the variables of interest. The comparison of results to surface observations and GPCC precipitation data also show that the modeled biases are reduced after the bias correction of the driving CESM data.

Our results show up to 2 K increases in winter mean T2 values, with a greater increase over the mountain ranges. Nearly 1 g/kg future increase in winter mean Qv2 values is projected for the entire model domain, and the biggest increase is projected to occur over the CV and along the California coast. The projected future changes in T2 and Qv2 values are statistically significant for almost all of California. A future decrease in winter mean daily maximum PBLH is observed for the entire model domain with greater magnitudes over the coastal areas and the arid region as compared to the rest of the state. The probability distributions of state-averaged winter Tmean, Tmax and Tmin show a shift of the means, 5th and 95th percentile to the warmer temperatures for all the three parameters. The distributions also show larger shifts of the left tails (cooler temperatures) than the right tails (warmer temperatures) towards the hotter end of the temperature distribution for all three parameters.

The projected future changes in winter mean precipitation show an increase of up to 50% over northern California and a decrease of up to 40% over southern California when compared to the current decade, which suggests that the relatively wet north would become wetter and the relatively dry south would become drier by the 2050s. As a result of the wintertime temperature rise, the solid phase precipitation (snow + graupel) is projected to decrease over the western side of the Sierra Nevada and the mountain ranges to the south of the central valley where the elevation is lower than 2000 m, despite an overall increase in total precipitation. The solid phase precipitation is projected to increase over the eastern side of the Sierra Nevada where the elevation is higher than 2000 m by the 2050s. Our results show a future reduction in the snow_to_precipitation ratio over most of the mountainous areas except for the eastern side of the Sierra Nevada (elevation higher than 2000 m), where the future change in snow_to_precipitation ratio is close to zero. The projected future changes in wintertime precipitation over California, together with the changes in snow over the mountain ranges, indicate substantial future variations in the snowpack and distribution over the Sierra Nevada, which is vital to California's water supply.

The influence of climate change on AR activities that approach the U.S. west coast is investigated by examining the IVT off the west coast. The results show a shift

Table 3 Number of days meeting each of the four thresholds, as well as all the four thresholds (All), for stagnation

	Stability	Near-surface wind	3000 feetwind	Precipitation	All
Current	704	491	596	951	202
Future	739	511	591	931	214

The data are averaged over SJV for the simulated current and future decades

of the peak of the ARs approaching the U.S. west coast from higher latitudes to California's northern and central coast (35° to 40° N) in the future decade, which is likely the reason for the projected future increase in wintertime precipitation over northern California.

The analysis on stagnation conditions over SJV, which is highly associated with the severe winter PM problem over this region, suggests an approximately 6% future increase in winter stagnant days over the SJV. This projected increase is shown to be attributed to more frequent occurrences of days with a more stably-stratified atmosphere and stagnant winds near the surface and at 3000 feet.

Our downscaled meteorological results with high spatiotemporal resolution provide references to policy makers in the environmental and water resources sectors to better understand how water supplies and wintertime air quality issues over California that may change by the 2050s under a changing climate. This will inform the development of strategies aimed at mitigating the effect of climate change on those aspects. We would like to point out that this work represents only a single future climate realization with fine resolution over California. Different assumptions in radiative forcing scenarios and different GCMs may result in different future realizations over this region, producing different future projections in regional meteorology and air quality. For instance, there can be considerable uncertainties in the wintertime circulation projection over the Californian coast from different GCMs and different emission scenarios. As the consequence, the future projection in precipitation can be different from this study when driven by a different GCM or/and a different radiative forcing scenario. Although we believe that the scenario selected in this study is more realistically aligned with the future green house gas emission reduction in California, and the bias correction applied to the CESM data in this study would reduce the uncertainty of the future projection to a certain extent, the downscaled results from this study still do not fully represent real future conditions and the consensus from other GCMs. CMIP5 multi-model ensemble could be used to further reduce the uncertainty of future projections, which will be pursued in our future studies.

References

Bao JW, Michelson SA, Persson POG, Djalalova IV, Wilczak JM (2008) Observed and WRF-simulated low-level winds in a high-ozone episode during the Central California ozone study. J Appl Meteorol Climatol 47:2372–2394

Berg N, Hall A (2015) Increased inter-annual precipitation extremes over California under climate change. J Clim 28:6324–6334. https://doi.org/10.1175/JCLI-D-14-00624.1

Berg N, Hall A (2017) Anthropogenic warming impacts on California snowpack during drought. Geophys Res Lett 44:2511–2518. https://doi.org/10.1002/2016GL072104

Caldwell P, Chin H-NS, Bader DC, Bala G (2009) Evaluation of a WRF dynamical downscaling simulation over California. Clim Change 95(3–4):499–521. https://doi.org/10.1007/s10584-009-9583-5

Chen J, Lu J, Avise JC, DaMassa JA, Kleeman MJ, Kaduwela AP (2014) Seasonal modeling of PM2.5 in California's San Joaquin Valley. Atmos Environ 92:182–190

Chen J et al (2020) Modeling air quality in the San Joaquin valley of California during the 2013 Discover-AQ field campaign. Atmos Environ 5:100067. https://doi.org/10.1016/j.aeaoa.2020.100067

Cordeira JM, Ralph FM, Moore BJ (2013) The development and evolution of two atmospheric rivers in proximity to western North Pacific tropical cyclones in October 2010. Mon Weather Rev 141:4234–4255. https://doi.org/10.1175/MWR-D-13-00019.1

Coumou D, Rahmstorf S (2012) A decade of weather extremes. Nat Clim Change 2:491–496. https://doi.org/10.1038/nclimate1452

Das T, Dettinger MD, Cayan DR, Hidalgo HG (2011) Potential increase in floods in Californian Sierra Nevada under future climate projections. Clim Change 109(suppl 1):S71–S94

Deser C, Terray L, Phillips AS (2016) Forced and internal components of winter air temperature trends over North America during the past 50 years: Mechanisms and implications. J Clim 29:2237–2258

Dettinger MD (2011) Climate change, atmospheric rivers and floods in California—A multi-model analysis of storm frequency and magnitude changes. J Am Water Resour Assoc 47:514–523. https://doi.org/10.1111/j.1752-1688.2011.00546.x

Dockery WD et al (1993) An association between air pollution and mortality in six US cities. N Engl J Med 329:1753–1759

Dudhia J (1989) Numerical study of convection observed during the winter monsoon experiment using a mesoscale two-dimensional model. J Atmos Sci 46:3077–3107

Eldering A, Cass GR (1996) Source-oriented model for air pollutant effects on visibility. J Geophys Res 101(D14):19343–19369. https://doi.org/10.1029/95JD02928

Gao Y, Lu J, Leung LR, Yang Q, Hagos S, Qian Y (2015) Dynamical and thermodynamical modulations on future changes of landfalling atmospheric rivers over western North America. Geophys Res Lett 42:7179–7186. https://doi.org/10.1002/2015GL065435

Gershunov A, Shulgina T, Clemesha RE, Guirguis K, Pierce DW, Dettinger MD, Lavers DA, Cayan DR, Polade SD, Kalansky J, Martin Ralph F (2019) Precipitation regime change in western North America: The role of atmospheric rivers. Sci Rep 9:9944. https://doi.org/10.1038/s41598-019-46169-w

Guan B, Waliser DE, Molotch NP, Fetzer EJ, Neiman PJ (2012) Does the Madden–Julian oscillation influence wintertime atmospheric rivers and snowpack in the Sierra Nevada? Mon Weather Rev 140:325–342

Ham WA, Herner JD, Green PG, Kleeman MJ (2010) Size distribution of health-relevant trace elements in airborne particulate matter during a severe winter stagnation event: implications for epidemiology and inhalation exposure studies. Aerosol Sci Technol 44:753–765

Held IM, Soden BJ (2006) Robust responses of the hydrological cycle to global warming. J Clim 19(21):5686–5699

Herner JD, Aw J, Gao O, Chang DP, Kleeman MJ (2005) Size and composition distribution of airborne particulate matter in northern California: I-particulate mass, carbon, and water-soluble ions. J Air Waste Manag Assoc 55:30–51

Herner JD, Ying Q, Aw J, Gao O, Chang DPY, Kleeman MJ (2006) Dominant mechanism that shape the airborne particle size and composition distribution in central California. Aerosol Sci Technol 40:827–844

Hong S-Y, Lim J-OJ (2006) The WRF single-moment 6-class microphysics scheme (WSM6). J Korean Meteorol Soc 42:129–151

Hong S-Y, Noh Y, Dudhia J (2006) A new vertical diffusion package with an explicit treatment of entrainment processes. Mon Weather Rev 134:2318–2341

Horton D, Diffenbaugh N (2012) Response of air stagnation frequency to anthropogenically enhanced radiative forcing. Environ Res Lett 7(4):044034. https://doi.org/10.1088/1748-9326/7/4/044034

Horton DE, Shinner CB, Singh D, Diffenbaugh NS (2014) Occurrence and persistence of future atmospheric stagnation events. Nat Clim Change 4(8):698–703. https://doi.org/10.1038/nclimate2272

Huang X, Hall AD, Berg N (2018) Anthropogenic warming impacts on today's Sierra Nevada snowpack and flood risk. Geophys Res Lett 45:6215–6222. https://doi.org/10.1029/2018GL077432

Huning LS, AghaKouchak A (2018) Mountain snowpack response to different levels of warming. Proc Natl Acad Sci 115(43):10932–10937

IPCC (2012) Managing the risks of extreme events and disasters to advance climate change adaptation. In: Field CB, Barros V, Stocker TF, Qin D, Dokken DJ, Ebi KL, Mastrandrea MD, Mach KJ, Plattner G-K, Allen SK, Tignor M, Midgley PM (eds) A special report of working groups I and II of the intergovernmental panel on climate change. Cambridge University Press, Cambridge

Jankov I, Bao J-W, Neiman PJ, Schultz PJ, Huiling Y, White AB (2009) Evaluation and comparison of microphysical algorithms in ARW-WRF model simulations of atmospheric river events affecting the California coast. J Hydrometeor 10:847–870

Kain JS (2004) The Kain–Fritsch convective parameterization: an update. J Appl Meteorol 43:170–181

Lavers DA, Villarini G, Allan RP, Wood EF, Wade AJ (2012) The detection of atmospheric rivers in atmospheric reanalyses and their links to British winter floods and the large-scale climatic circulation. J Geophys Res 117:D20106. https://doi.org/10.1029/2012JD018027

Leung LR, Gustafson WI Jr (2005) Potential climate change and implications to US air quality. Geophys Res Lett 32:L16711. https://doi.org/10.1029/2005GL022911

Leung LR, Qian Y (2009) Atmospheric rivers induced heavy precipitation and flooding in the western US simulated by the WRF regional climate model. Geophys Res Lett 36:L03820. https://doi.org/10.1029/2008GL036445

Lu W, Zhong S, Charney JJ, Bian X, Liu S (2012) WRF simulation over complex terrain during a southern California wildfire event. J Geophys Res 117:D05125. https://doi.org/10.1029/2011JD017004

Meehl GA et al (2007) Global climate projections. In: Solomon S et al (eds) Climate change 2007: the physical science basis. Cambridge University Press, pp 747–845

Meehl GA et al (2000) An introduction to trends in extreme weather and climate events: Observations, socioeconomic impacts, terrestrial ecological impacts, and model projections. Bull Am Meteor Soc 81:413–416

Meehl GA, Washington WM, Arblaster JM, Hu A, Teng H, Tebaldi C, Strand WG, White JB III (2012) Climate system response to external forcings and climate change projections in CCSM4. J Clim 25:3661–3683

Mesinger F, DiMego G, Kalnay E, Mitchell K et al (2006) North American regional reanalysis. Bull Am Meteorol Soc 87:343–360. https://doi.org/10.1175/BAMS-87-3-343

Mlawer EJ, Taubman SJ, Brown PD, Iacono MJ, Clough SA (1997) Radiative transfer for inhomogeneous atmospheres: RRTM, a validated correlated-k model for the longwave. J Geophys Res 102:16663–16682. https://doi.org/10.1029/97JD00237

Neiman PJ et al (2008a) Diagnosis of an intense atmospheric river impacting the Pacific Northwest: storm summary and offshore vertical structure observed with COSMIC satellite retrievals. Mon Weather Rev 136(11):4398–4420. https://doi.org/10.1175/2008MWR2550.1

Neiman PJ, Ralph FM, Wick GA, Lundquist JD, Dettinger MD (2008b) Meteorological characteristics and overland precipitation impacts of atmospheric rivers affecting the West Coast of North America based on eight years of SSM/I satellite observations. J Hydrometeorol 9(1):22–47. https://doi.org/10.1175/2007JHM855.1

Peacock S (2012) Projected twenty-first-century changes in temperature, precipitation, and snow cover over North America in CCSM4. J Clim 25:4405–4429. https://doi.org/10.1175/JCLI-D-11-00214.1

Pierce DW, Das T, Cayan DR et al (2013) Probabilistic estimates of future changes in California temperature and precipitation using statistical and dynamical downscaling. Clim Dyn 40:839–856. https://doi.org/10.1007/s00382-012-1337-9

Pleim JE, Xiu A (1995) Development and testing of a surface flux and planetary boundary layer model for application in mesoscale models. J Appl Meteorol 34:16–32

Polade SD, Gershunov A, Cayan DR, Dettinger MD, Pierce DW (2017) Precipitation in a warming world: assessing projected hydro-climate changes in California and other Mediterranean climate regions. Sci Rep 7:10783. https://doi.org/10.1038/s41598-017-11285-y

Pope CA III, Dockery DW (2006) Health effects of fine particulate air pollution: lines that connect. J Air Waste Manag 56:709–742

Ralph FM, Dettinger MD (2011) Storms, floods, and the science of atmospheric rivers. Eos Trans AGU 92(32):265. https://doi.org/10.1029/2011EO320001

Ralph FM, Dettinger MD (2012) Historical and national perspectives on extreme West Coast precipitation associated with atmospheric rivers during December 2010. Bull Am Meteorol Soc 93:783–790. https://doi.org/10.1175/BAMS-D-11-00188.1

Ralph FM, Neiman PJ, Wick GA, Gutman SI, Dettinger MD, Cayan DR, White AB (2006) Flooding on California's Russian River: role of atmospheric rivers. Geophys Res Lett 33:L13801. https://doi.org/10.1029/2006GL026689

Rutz JJ, Steenburgh WJ, Ralph FM (2014) Climatological characteristics of atmospheric rivers and their inland penetration over the western United States. Mon Weather Rev 142:905–921. https://doi.org/10.1175/MWR-D-13-00168.1

Skamarock WC, Klemp JB, Dudhia J, Gill DO, Barker DM, Wang W, Powers JG (2008) A description of the advanced research WRF version 3. NCAR Tech. Note NCAR/TN-4751STR

Swain DL, Tsiang M, Haugen M, Singh D, Charland A, Rajaratnam B, Diffenbaugh NS (2014) The extraordinary California drought of 2013/2014: character, context, and the role of climate change. Bull Am Meteorol Soc 95(9):S3–S7

Swain DL, Langenbrunner B, Neelin JD et al (2018) Increasing precipitation volatility in twenty-first-century California. Nat Clim Change 8:427–433. https://doi.org/10.1038/s41558-018-0140-y

Taylor KE, Stouffer RJ, Meehl GA (2012) An overview of CMIP5 and the experiment design. Bull Am Meteor Soc 93:485–498. https://doi.org/10.1175/BAMS-D-11-00094.1

Ullrich PA, Xu Z, Rhoades AM, Dettinger MD, Mount JF, Jones AD, Vahmani P (2018) California's drought of the future: a midcentury recreation of theexceptional conditions of 2012–2017. Earth's Future 6:1568–1587. https://doi.org/10.1029/2018EF001007

Wang JXL, Angell JK (1999) Air stagnation climatology for the United States (19481998) (NOAA/Air Resources Laboratory ATLAS No. 1. 1999)

Wang SYS, Yoon J-H, Becker E, Gillies R (2017) California from drought to deluge. Nat Clim Change 7:465–468

Warner MD, Mass CF, Salathé EP (2015) Changes in winter atmospheric rivers along the North American west coast in CMIP5 climate models. J Hydrometeorol 16(1):118–128

Xu Z, Yang Z-L (2012) An improved dynamical downscaling method with GCM bias corrections and its validation with 30 years of climate simulations. J Clim 25(18):6271–6286

Xu Z, Yang Z-L (2015) A new dynamical downscaling approach with GCM bias corrections and spectral nudging. J Geophys Res Atmos 120:3063–3084. https://doi.org/10.1002/2014JD022958

Zhao Z, Chen S-H, Kleeman MJ, Tyree M, Cayan D (2011a) The impact of climate change on air quality-related meteorological conditions in California. Part I: present time simulation analysis. J Clim 24:3344–3361. https://doi.org/10.1175/2011JCLI3849.1

Zhao Z, Chen SH, Kleeman MJ, Mahmud A (2011b) The impact of climate change on air quality–related meteorological conditions in California. Part II: Present versus future time simulation analysis. J Clim 24:3362–3376. https://doi.org/10.1175/2010JCLI3850.1

Zhao Z, Di P, Chen S et al (2020) Assessment of climate change impact over California using dynamical downscaling with a bias correction technique: method validation and analyses of summertime results. Clim Dyn. https://doi.org/10.1007/s00382-020-05200-x